



# Molecular simulation of methane adsorption in micro- and mesoporous carbons with applications to coal and gas shale systems



Keith Mosher, Jiajun He, Yangyang Liu, Erik Rupp, Jennifer Wilcox \*

Department of Energy Resources Engineering, School of Earth Sciences, Stanford University, Green Earth Sciences 065, 367 Panama Street, Stanford, CA 94305, United States

## ARTICLE INFO

### Article history:

Received 6 September 2012

Received in revised form 30 December 2012

Accepted 2 January 2013

Available online 18 January 2013

### Keywords:

Methane adsorption

Excess adsorption

Coal-bed methane

Enhanced gas recovery

Enhanced coal-bed methane recovery

Grand canonical Monte Carlo

## ABSTRACT

Methane adsorption in porous carbon systems such as coal and the organic matrix of gas shales is an important factor in determining the feasibility of CO<sub>2</sub> injection for enhanced natural gas recovery and possible sequestration of CO<sub>2</sub>. Methane and CO<sub>2</sub> adsorb competitively on carbon surfaces and an understanding of each gas individually is important for determining a model to predict the feasibility of this approach for permanent CO<sub>2</sub> storage. Coal and gas shales have a very heterogeneous pore system, ranging from the micro, meso, and macro-scales, with the pore size strongly affecting the adsorption behavior. In micropores, the force fields of opposing pore walls are close enough that they will overlap and significantly influence the adsorption behavior, which affects adsorbate packing and density. To determine the size at which these effects become non-negligible and to determine the magnitude of this impact, grand canonical Monte Carlo simulations have been carried out to estimate the adsorption isotherms of methane across a range of pore sizes and at various temperature and pressure conditions characteristic of subsurface conditions. These isotherms have been calculated on graphitic surfaces as an initial model of coal and kerogen of gas shales. The general trend within pore sizes is that larger pores exhibit lower excess density compared to smaller pores. However, at pressure above 1 MPa, the adsorption capacities of 0.6-nm pores drop below those of the wider pores, ultimately decreasing below that of the 1.2-nm pore at 18 MPa. The density of adsorbed methane changes non-monotonically with increasing pore width, and drops to a minimum in 1.2-nm pores at 12 MPa. The isotherms have been compared with experimental data to gauge their accuracy, and the behavior of the adsorbed layer has been examined in detail. At pressures less than 2.5 MPa, the molecular simulation estimates underpredict the excess adsorption, while at pressures greater than 2.5 MPa up to 20 MPa, the simulation estimates overpredict the excess adsorption. This discrepancy is likely due to the limitation of the experimental-based model that was used to generate the pore size distribution and the surface functionalities of the porous media that were ignored in the molecular simulation investigations, but likely play an important role in determining accurate capacities under confinement at the nanoscale.

© 2013 Elsevier B.V. All rights reserved.

## 1. Introduction

Currently, global CO<sub>2</sub> emissions from the energy sector are approximately 30 billion tons per year with this number expected to double by 2050 under business-as-usual practices (IEA, 2010). It has been estimated that to stabilize CO<sub>2</sub> levels in the atmosphere, they will have to be reduced by up to 85% over the next century and to do this requires a reduction of approximately 20 billion tons of CO<sub>2</sub> each year (Davis et al., 2010; Hoffert et al., 2002). Carbon capture and sequestration (CCS) has the potential to reduce emissions by up to 5–10 billion tons per year with a minimum storage capacity of up to 2000 billion tons in geologic formations (Benson and Orr, 2008). With fossil fuels representing 80% of global energy production, it is clear that CCS must be a component of the portfolio for mitigating global CO<sub>2</sub> emissions. Storage capacities of unmineable coalbeds are

estimated to range between 100 and 300 Gt CO<sub>2</sub>. This is low compared to the potential storage capacity of deep saline aquifers (i.e., 1000–10,000), but there are incentives with storage in unmineable coalbeds as it may allow for enhanced coalbed methane recovery (ECBM) (Wilcox, 2012). A similar approach of using CO<sub>2</sub> for enhanced methane recovery from gas shales may also lead to advancements in the technological feasibility of storing CO<sub>2</sub> in depleted shale reservoirs. Significant effort has been made to develop an understanding of CBM (Moore, 2012) and ECBM processes using CO<sub>2</sub> (Busch and Gensterblum, 2011). Coal and the organic matrix of gas shales are heterogeneous materials both physically, in terms of their pore size, structure and connectivity, and chemically, in terms of the pore surface functional groups. The petrographic composition of coals has been investigated for methane sorption previously, and indicates that vitrinite-rich coals have a greater capacity for methane than inertinite-coals, likely due to the microporosity associated with vitrinite (Chalmers and Bustin, 2007). Similar analyses of gas shales link increases in total organic content (TOC)

\* Corresponding author. Tel.: +1 650 724 9449; fax: +1 650 725 2099.  
E-mail address: [wilcoxj@stanford.edu](mailto:wilcoxj@stanford.edu) (J. Wilcox).

and micropore volume (related to TOC) to increased methane adsorption (Ross and Bustin, 2009; Zhang et al., 2012).

Understanding the adsorption of methane in micro- and mesoporous carbon has practical application in both the recovery of methane from subsurface coal and gas shales, as well as the sequestration of CO<sub>2</sub> in the gas-depleted pore space of each of these systems. Enhanced natural gas recovery processes address not only the increasing importance of natural gas for energy security, but also the increasing awareness of and concern regarding the role of CO<sub>2</sub> as a greenhouse gas.

Capacity estimation based upon adsorption has consistently been one of the most valuable and important topics of this field (Heuchel et al., 1999). High-level trends affecting the adsorption quantity are sorbent chemical composition, porosity, pore size distribution, temperature, and pressure. For ECBM applications, simulations and experiments have demonstrated that CO<sub>2</sub> will preferentially adsorb in pores over methane (Cracknell et al., 1996; Dreisbach et al., 1999; Kurniawan et al., 2006). In a recent study by Liu and Wilcox, it was shown that the selectivity of CO<sub>2</sub> over CH<sub>4</sub> is approximately five when the gas mixture is adsorbed in slit pores containing oxygen functional groups at temperature and pressure conditions relevant to ECBM applications (Liu and Wilcox, 2012a). This has the beneficial effect whereby adsorbed methane is displaced by CO<sub>2</sub>, releasing more methane than could be accessed through the use of standard recovery techniques. Separation processes continue to be improved as additional selectivity simulations, such as methane and ethane in carbon slit pores, are carried out (Cracknell et al., 1994). An additional concern for ECBM practices is the impact of H<sub>2</sub>O (typically present in coal) on methane and CO<sub>2</sub> adsorption. Simulations suggest that for micropores (i.e., <2 nm), water may prevent a significant percentage of methane adsorption that would otherwise occur (Müller and Gubbins, 1998; Müller et al., 1996, 2000).

In the current work, molecular simulations have been carried out using a grand canonical Monte Carlo (GCMC) algorithm (Allen, 1989; Frenkel, 2001) to predict the adsorption isotherms for carbon-based slit pores of a given width, spanning both micro and mesoporous regimes. There are many complex aspects that may influence adsorption, including pore surface functional groups, water interference, and surface irregularities; however, to isolate the influence of pore size on adsorption phenomena, we adopt a simplified model of these complex porous carbon-based systems using an ideal graphite-based simulation cell. The primary force considerations for adsorption include the interactions between gas molecules and the pore surfaces, neighboring pore wall interactions, as well as the interactions between the gas molecules themselves either in a free gas state or adsorbed state. However, it can be inferred that for a specific pore size, in particular nearing the molecular dimensions of the adsorbing gas, the forces from the opposing walls will be more significant as well as forces from the neighboring molecules adsorbed to the pore walls. There are two primary factors in a given coal or shale sample that changes with the pore size distribution (PSD), which may significantly affect adsorption. These are the surface area associated with the pore walls and the overlapping force fields by

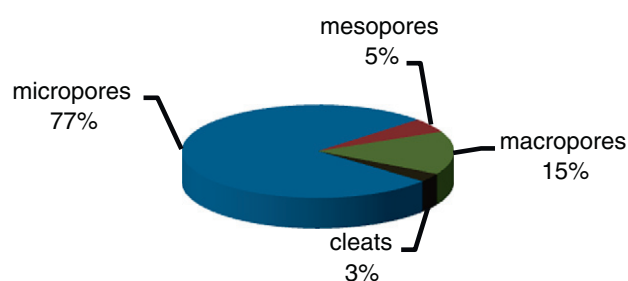


Fig. 1. Pore size distribution in a bituminous coal from the Illinois Basin (Mardon, 2008).

opposing walls in sufficiently narrow pores. How these factors affect adsorption is not straightforward, and is not well documented in the literature. To improve understanding of adsorption in such systems and to create more reliable predictions of adsorption behavior, we have investigated via molecular simulation, adsorption phenomena over a wide range of pore sizes, for various temperature and pressure conditions applicable to subsurface applications. The goal of the current study is to characterize the effect of pore size on methane adsorption and to quantify this impact to improve understanding of methane adsorption in micro and mesoporous carbon systems for natural carbon-based systems.

## 2. Adsorption terminology

Coal and gas shales are complex systems that contain carbon-based 3D pore networks with a significant amount of surface area contained in the micropores as demonstrated in Fig. 1. Based upon the IUPAC (International Union of Pure and Applied Chemistry) definition, a micropore is defined as a pore having a width of less than 2 nm, while a mesopore is defined as having a width between 2 and 50 nm (Sing et al., 1985).

Examples of various pore size distributions from a variety of coals (Gan et al., 1972) and three shales investigated in the current work are shown in Table 1. The parameters V<sub>1</sub>, V<sub>2</sub> and V<sub>3</sub> were defined in the earlier study carried out in 1972 as the fractions of pore volumes with diameters greater than 30 nm, between 1.2 nm and 30 nm, and less than 1.2 nm, respectively. Although the definition between micro-, meso- and macropores in the earlier study is different than the current IUPAC definitions, this example provides insight into the relationship between the pore size of a given coal and its rank. For instance, in the case of anthracite, a high-rank coal, at least 75% of the pore volume is dominated by micropores, which is consistent with Fig. 1. In the case of lignite, a low-rank coal, the majority of the pore volume is dominated by macropores in all three of the samples investigated.

It is important to note that determining the percentage of pore volume in the micro- versus mesopore domains depends upon the probe gas used. For instance, it is well-known that N<sub>2</sub> and Ar are non-adsorbing gases, but that CO<sub>2</sub> in porous carbons has the propensity to adsorb. These properties may influence gas uptake in the pores and in the case of using CO<sub>2</sub>, may lead to overestimates of the pore volume since the density of CO<sub>2</sub> is likely greater than it would be in

Table 1  
Pore volume percentages of coals (Gan et al., 1972) and shales (current work).

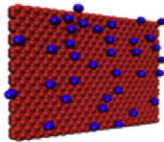
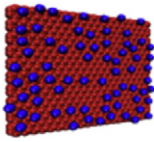
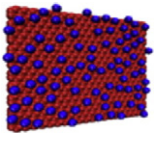
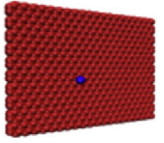
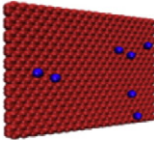
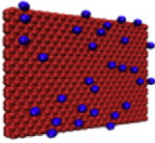
Sample	Rank	V <sub>3</sub> (%) <1.2 nm	V <sub>2</sub> (%) 1.2–30 nm	V <sub>1</sub> (%) >30 nm
<i>Coals<sup>a</sup></i>				
PSOC-80	Anthracite	75.0	13.1	11.9
PSOC-127	LV bit.	73.0	~0	27.0
PSOC-135	MV bit.	61.9	~0	38.1
PSOC-4	HVA bit.	48.5	~0	51.5
PSOC-105A	HVB bit.	29.9	45.1	25.0
Rand	HVC bit.	47.0	32.5	20.5
PSOC-26	HVC bit.	41.8	38.6	19.6
POC-197	HVB bit.	66.7	12.4	20.9
PSOC-190	HVC bit.	30.2	52.6	17.2
PSOC-141	Lignite	19.3	3.5	77.2
PSOC-87	Lignite	40.9	~0	59.1
PSOC-89	Lignite	12.3	~0	87.7
<i>Shales<sup>b</sup></i>				
Eagleford	–	7.7/7.7	45.4/50.9	46.9/41.4
Haynesville	–	11.9/9.5	41.9/45.4	46.2/45.2
Barnett	–	10.0/7.7	46.7/47.5	43.3/44.8

<sup>a</sup> LV = low-volatile bituminous coal; MV = medium-volatile bituminous coal; HVA, HVB and HVC bit. = high-volatile bituminous coal rank A, B and C, respectively;

<sup>b</sup> Two numbers indicate results from adsorption of two probe gases, i.e., N<sub>2</sub> or Ar.

**Table 2**

3D snapshots of slices through adsorbed and bulk phases at 298 K in a 2-nm pore; red = surface carbon atoms and blue = methane molecules.

	1 MPa	6.2 MPa	18 MPa
Adsorbed			
Bulk			

a traditional condensed liquid phase. The different pore sizes can also be expected to exhibit different pore filling (adsorption) mechanisms as pressure increases. For instance, micropores will experience primarily physisorption at a pore-filling stage only, whereas meso and macropores will undergo two stages of adsorption, first with single and multilayer adsorption, and second, capillary condensation (Lowell, 2004; Wilcox, 2012). In micropores, adsorption is governed by combined gas-surface and gas-gas interactions, and thus is limited to a single layer or very few condensed molecular layers. In many cases the density of the adsorbed (condensed) phase is even higher than that of the liquid density. The micropores reflect a continuous filling process due to the overlapping forces of the pore walls, which differs from pore condensation representative of a gas-liquid phase transition that takes place in mesopores.

One of the challenges in evaluating adsorption behavior is differentiating between the number of gas molecules that would fill a given volume in the absence of pore walls versus the number of molecules that would fill that same volume, but with the inclusion of pore-wall effects at the same temperature and pressure conditions. In other words, in micropores and smaller mesopores, the gas in the pore will experience interactions with the pore walls that will influence adsorption properties such as packing and density. There are several terms that are used in the literature to characterize adsorption, i.e., *total gas content*, *absolute*, and *excess* adsorption.

Before defining these terms it is important to first understand how one determines the volume a gas occupies at a given temperature and pressure in the absence of pore walls, which is termed the *bulk* phase. When carrying out molecular simulations for predicting adsorption, densities are calculated as a function of fugacity rather than pressure, with fugacity loosely defined as the deviation in the vapor pressure exerted by a real gas from the corresponding ideal gas. Within the current work, the fugacity (i.e., 'corrected' pressure) is calculated using the Peng–Robinson equation of state (Eq. (1)), with this pressure used in plotting the adsorption isotherms.

$$p = -\frac{RT}{V_m - b} - \frac{a\alpha}{V_m^2 + 2bV_m - b^2} \quad (1)$$

such that:

$$a = \frac{0.457235R^2T_c^2}{P_c},$$

$$b = \frac{0.077796RT_c}{P_c},$$

$$\alpha = \left(1 + \kappa(1 - T_r^{0.5})\right)^2,$$

$$\kappa = 0.37464 + 1.54226\omega - 0.26992\omega^2,$$

$$T_r = \frac{T}{T_c}.$$

such that  $T_c$ ,  $p_c$ , and  $\omega$  are the critical temperature, critical pressure and acentric factor, respectively.

*Total gas content* is defined as the entire quantity of gas that resides in the pore space at a given temperature and pressure and includes both the gas in the center of the pore (i.e., 'free' gas) as well as the gas adsorbed directly to the pore surface. Defining the boundary at which the gas is 'free' in the pore versus adsorbed to the surface is difficult, but more easily done with molecular simulation than with experiments. Given a large enough pore with minimal influence of the pore walls, the free gas in the pore center may be thought of as the gas that occupies the same volume of space at a given temperature and pressure as it would in its bulk phase. Theoretically, the free gas is not influenced by the pore walls, or any differently by its neighboring gas molecules as it would be in its bulk phase.

*Absolute adsorption* is defined as the quantity of gas present only in an adsorbed state. This metric is challenging because of the difficulty in identifying the molecules that are in fact adsorbed and not 'free' in the pore space. In practice this information must include the density of the adsorbed layer, single or multi-layer characteristics, and the overall surface area associated with a given pore volume. This term is often calculated based upon the assumption that the density in the adsorbed layer is equal to the liquid-phase density, which is often an incorrect assumption, especially with adsorbing gases at high pressures and in small pores.

*Excess adsorption* is defined as the additional amount of gas adsorbed per unit pore volume compared with the amount of gas in the same volume of a given pore in the absence of pore walls. Gas in the adsorbed phase is higher in density than the same gas in the bulk phase, so subtraction of the expected density of gas in the bulk from the total adsorption yields the additional density of gas in the system as a result of adsorption.

Table 2 contrasts two volumetric slices of a 2-nm pore, showing all gas molecules between a wall of graphite and the center of a graphitic pore. In the case of the bulk phase, the wall is present only for comparison and its effect is not included in the simulation. Pressure conditions of 1, 6.2, and 18 MPa are shown. Even at the highest pressure, the density difference between the bulk and adsorbed phases is significant, and at lower pressures the adsorbed density is clearly higher than the bulk-phase density. It is worth noting that, while the density of the adsorbed phase is much higher, the pressure increase changes

**Table 3**  
Potential parameters for force field calculations.

	$\epsilon_{ff}/k_B$ (K)	$\sigma_{ff}$ (nm)
CH <sub>4</sub> <sup>a</sup>	148	0.375
C (graphite) <sup>b</sup>	28	0.34

<sup>a</sup> Ref (Martin and Siepmann, 1998);

<sup>b</sup> Ref (Steele, 1973).

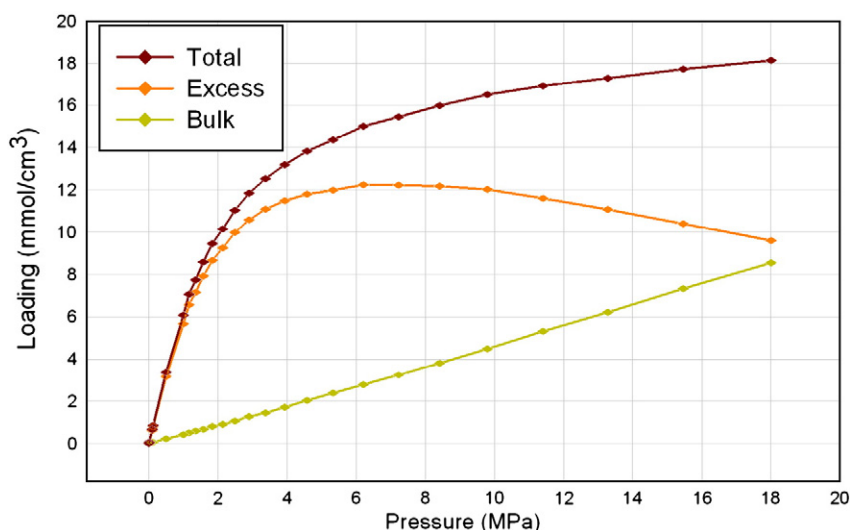


Fig. 2. Adsorption isotherm for total, excess and bulk adsorption of methane in a 1-nm pore at 298 K over a pressure range of 0.01 to 18 MPa.

the number of particles in the bulk from 1 to 7 and then 30, but in the adsorbed layer the number increases from 36 to 72 and finally 90. The rate of increase, and even the number of molecules added from a pressure increase of 6.2 to 18 MPa is greater in the bulk phase than in the adsorbed phase.

### 3. Theoretical methodology

In the current work, GCMC simulations have been carried for the prediction of methane adsorption in carbon-based systems at temperature and pressure conditions relevant to applications of enhanced gas recovery and permanent storage of CO<sub>2</sub> in coal and gas shales. Complex porous carbon structures have been modeled ideally as a collection of independent, non-interconnected, graphitic slit pores as a first step. Within the molecular simulations, each pore wall is represented using a 3-layer perfect graphite slab. The GCMC simulation box containing a given slit pore has dimensions of 4.272 × 4.932 nm in the x- and y-directions, respectively and with periodic boundary conditions. The distance between the two slabs in the z-direction was adjusted to model the various widths of the slit pores.

To describe the adsorption of methane in carbon-based slit pores, methane was treated simply as a one-center Lennard–Jones (12–6) sphere due to the fact that methane has a relatively weak octupole moment (Martin and Siepmann, 1998). To reduce the computational time, a rigid graphite framework was assumed, which is based on the fact that the geometries of the framework were not significantly influenced by methane adsorption. The LJ 12–6 parameters for the slit-pore surface carbon atoms were taken from the Steele 10–4–3 potential (Steele, 1973). As shown in Table 3, the ratio  $\epsilon_{ff}/k_B$  is the depth of the potential well, and  $\sigma_{ff}$  is the finite distance at which the intermolecular potential is zero. The potential energies associated with different Leonard-Jones sites were calculated using standard Lorentz–Berthelot mixing rules (Allen, 1989).

The GCMC simulations (Allen, 1989; Frenkel, 2001) of methane adsorption on perfect graphitic slit pores were carried out in the  $\mu VT$  ensemble (Gupta et al., 2003). Temperatures of 298 K, 318 K and 332 K, and pressures up to 20 MPa have been investigated for their relevance to CCS applications. The fugacities are required simulation inputs and as previously discussed were calculated using the Peng–Robinson equation of state (Reid et al., 1987). The critical temperature and pressure of methane are 190.4 K and 4.6 MPa, respectively, with

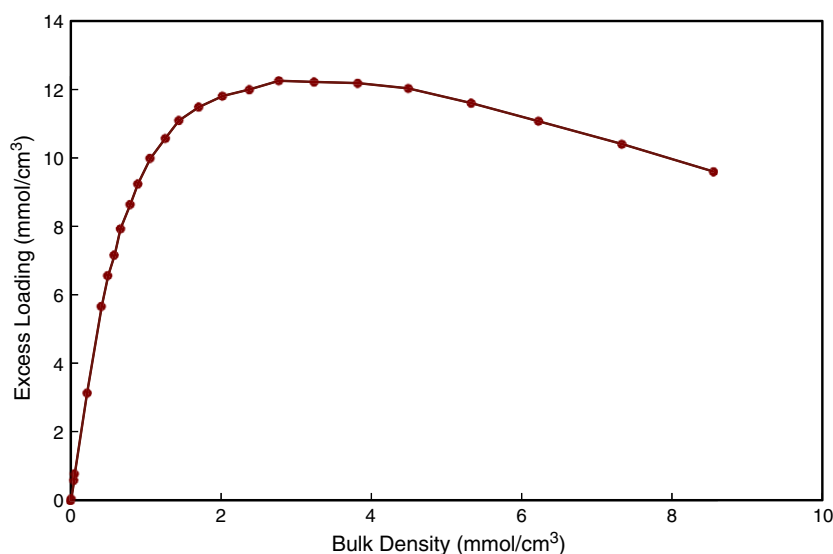


Fig. 3. Excess loading as a function of bulk density of methane in a 1-nm pore at 298 K.

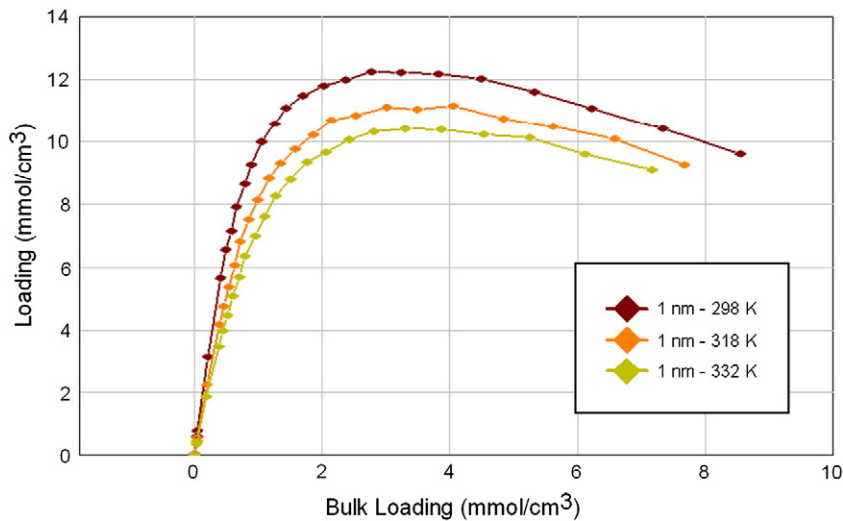


Fig. 4. Adsorption isotherms of methane adsorption in a 1-nm pore at temperatures of 298 K, 318 K and 332 K.

an acentric factor of 0.011. To speed up the convergence, energy-biased insertions of the gas molecules were employed and acceptance ratios for insertions and deletions were above 1% (slightly lower at higher loadings) to ensure reasonable equilibration in the GCMC simulations. A total of 100 million GCMC moves were attempted during each GCMC simulation.

#### 4. Results and discussion

##### 4.1. Isotherm predictions as a function of pressure and temperature

Fig. 2 shows the predicted isotherm for the total gas content, bulk and excess adsorption of methane in a 1-nm pore at 298 K and over a pressure range of 0.01 to 18 MPa. Adsorption creates a layer of gas at a higher density near the pore surface than would be expected from a gas in its bulk phase without a nearby surface at the same temperature and pressure. Subtracting the bulk from the total gas content, the additional methane density (i.e., excess) attributed to surface

effects can be seen in Fig. 2. The pore volume was calculated by assuming that the effective pore width is equal to the distance between the two graphitic slabs minus the collision diameter of a surface carbon atom (i.e., 0.34 nm). The pore volume is typically determined using helium as the probe gas at ambient temperature before initiating adsorption experiments, and in the molecular simulation investigations of the current work helium is used in a similar manner to determine the reference pore volume (Liu and Wilcox, 2012b).

With sufficient pressure increase, most systems reach a point where the adsorbed state has a density identical to that of the bulk phase and at this point the total and bulk isotherms intersect. The amount of excess therefore increases up to a specific pressure, and then decreases to zero at the pressure for which there is no noticeable change in density as a result of adsorption. The increase with pressure followed by a subsequent decrease suggests there exists a maximum adsorbed quantity, or a layering of adsorbed molecules up to a certain distance from the pore wall. The increase corresponds to the many available locations within the adsorbed layer, up to the peak of the

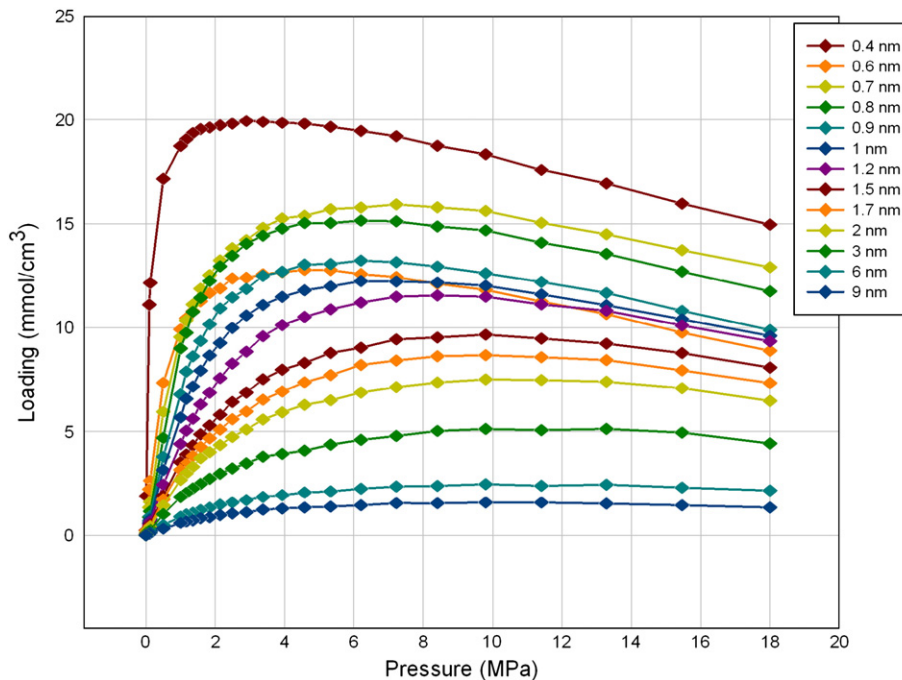


Fig. 5. Excess adsorption isotherms at 298 K in slit pores with pore sizes ranging from 0.4 nm to 9 nm.

**Table 4**  
Maximum excess adsorption at 298 K in pores of sizes ranging from 0.4 nm to 9 nm.

Pore size (nm)	Pressure (MPa)	Loading (mmol/cm <sup>3</sup> )
0.4	2.900	19.94
0.6	4.578	12.79
0.7	7.226	15.92
0.8	6.206	15.15
0.9	6.206	13.23
1.0	6.206	12.25
1.2	8.413	11.56
1.5	9.795	9.66
1.7	9.795	8.67
2.0	9.795	7.50
3.0	13.27	5.12
6.0	9.795	2.47
9.0	9.795	1.60

isotherm, at which point all of the “easily available” sites become filled.

As pressure (and hence fluid density) continues to increase, the available adsorption sites in the adsorbed layer(s) fill up, until the additional pressure required to add another adsorbed molecule is equal to the pressure needed to add one more molecule to the bulk phase, from which point there are no more molecules added to the adsorbed state. As pressure increases with no additions to the adsorbed layer, the density in the bulk phase increases. Because no molecules are added into the adsorbed layer, the relative difference in the density decreases, following the isotherm down to zero, where the bulk density is identical to the adsorbed density and thus there is no gain as a result of adsorption. This behavior can create misleading or confusing artifacts in the isotherms, but by graphing the excess as a function of the bulk density at the same pressure, as shown in Fig. 3, trends can be reliably identified up to very high pressures.

To examine the effect that temperature has on methane adsorption in carbon slit pores, the same isotherms calculated at different temperatures are compared in Fig. 4. The results show similar trends, except that at higher temperatures a reduced density increase due to adsorption takes place at lower pressures. Excess density also peaks later, causing an intersection or greatly diminished distance between the curves for different temperatures, implying that higher temperature reduces adsorption for equivalent pressures, but the maximum

number of adsorbed molecules remains constant. As pressure increases at higher temperatures, the pores still have space available in the adsorbed layer, causing the isotherm to peak and descend at higher pressures than for the same sized pores at lower temperatures.

#### 4.2. Isotherm prediction based upon pore size

Fig. 5 shows excess methane adsorption as a function of pore size. Several interesting features and patterns are apparent from these isotherms. The general trend among the varying pore sizes is that the larger pores have a lower excess adsorption density than the smaller pores. Smaller pore sizes also reach their excess adsorption density peak at lower pressures and have that density decrease at a greater rate than larger pore sizes. Although not shown, adsorption as a function of temperature was also investigated. It was found that increased temperature causes a lower peak in excess adsorption density, but with a shift to higher pressure. At higher temperatures the excess adsorption density also diminishes less rapidly as pressure increases beyond the peak exhibited at lower temperatures.

Table 4 demonstrates this, listing the maximum adsorption for each pore size and the pressure at which it occurs. The smaller pores peak clearly and at very low pressures whereas the larger pores have a flatter and more indeterminate peak, but at higher pressures. The 0.4-nm pore shows a density resulting from adsorption that is nearly 20 times the bulk density at 2 MPa, whereas within a 9.0-nm pore, the excess density has diminished to only a small fraction of the bulk density at all pressures considered. For the largest pore sizes (i.e., 2, 3, 6, and 9 nm) the loading curve is very flat neighboring the maximum. This makes the actual “maximum” value not as instructive as it is for the smaller pores. The maximum value for the 3-nm pore, for example, appears to occur at a much higher pressure than for the 2-, 6- and 9-nm pores. For all 4 pore sizes, however, the difference in the loading between 8 and 16 MPa is very small (i.e., <1%).

The trends discussed in the current work agree with the concept of an adsorption layer with some maximum thickness. The pores that are 1.2 nm or less show additional curvature around the maximum loading point as well as demonstrating more excess adsorption than suggested by simple layering. This effect is significantly pronounced in smaller pores, suggesting a direct pore size effect on the adsorption layer thickness. A few notable exceptions to the trends raise some interesting questions. Note that the isotherm of the

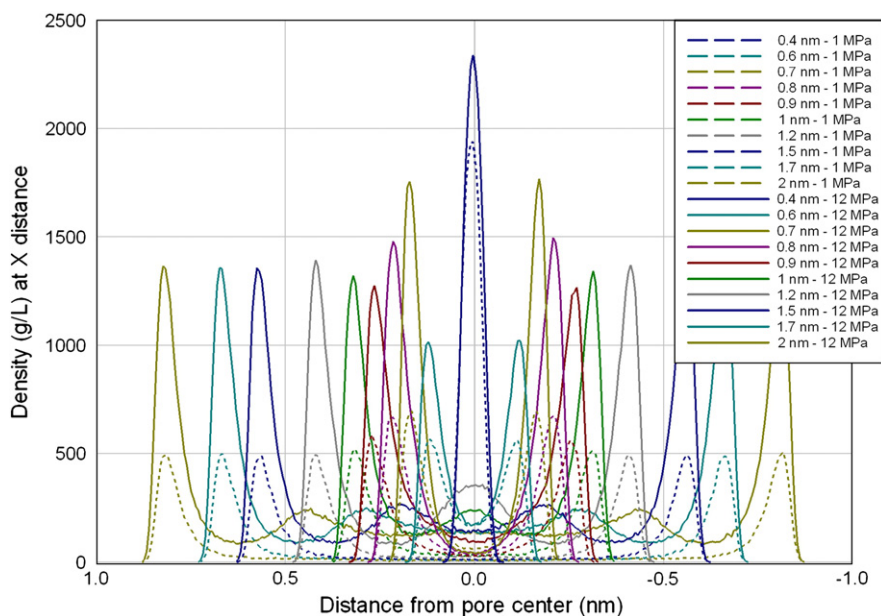


**Fig. 6.** Density profiles of the adsorbate molecules along the pores with pore diameters ranging from 0.4 nm to 2 nm at 1 MPa and 12 MPa.

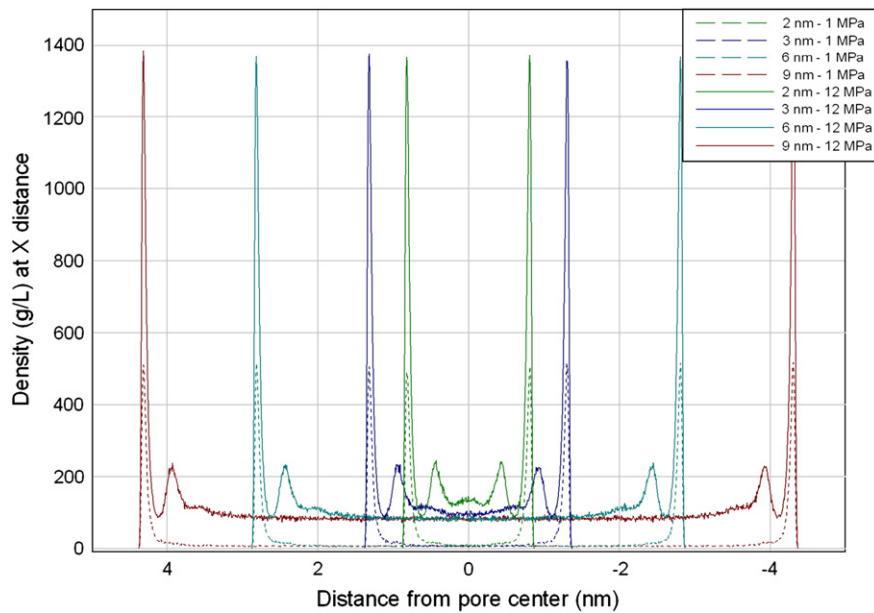


Fig. 7. Density profiles of the adsorbate molecules along the pores with pore diameters ranging from 2 nm to 9 nm at 1 MPa and 12 MPa.

0.6-nm pore does not conform to the pattern shown. The behavior is as expected at very low pressures, but above 1 MPa, the isotherm drops below those of the wider pores, ultimately decreasing below the isotherm of the 1.2-nm pore. To describe this phenomenon it is important to consider the Lennard–Jones diameter of methane (or the distance at which repulsive forces two molecules of methane dominate) when examining very small sized pores. This collision diameter, or  $\sigma$ , is 0.3751 nm for methane in these simulations. The 0.4-nm sized pores hold only one single molecular layer between two pore walls, while an 0.8-nm sized pore may hold up to two layers, one adsorbed to each wall; however, the formation of a layer on one wall of the 6- and 7-nm sized pores will interfere with the formation of a second layer on the opposing pore wall and therefore the change of the adsorption layers with the increase of pore width is not monotonic. The result is that, despite a pore volume increase from the 0.4-nm pore, and despite having more actual molecules in

place than found in the 0.4-nm pore, the density increase per unit volume increase is significantly less than that between the isotherms of the 0.4- and 1.2-nm pores. Furthermore, note that the isotherm of the 0.6-nm pore resembles a smaller version of the isotherm of the 0.4-nm pore, suggesting a single adsorbed layer rather than the rounder arc seen in the 0.8-nm isotherm, corresponding to double layering. The non-monotonic behavior was also reported in the molecular simulation work of Liu and Wilcox on CO<sub>2</sub> adsorption by employing the one-center Lennard-Jones model (Liu and Wilcox, 2012b).

#### 4.3. Density predictions of adsorbed methane

One of the challenges in adsorption experiments is that it is difficult to directly probe the adsorbed phase in small pores. This forces experimentalists to make assumptions about the layering and density of the adsorbed state. The typical assumption is that the adsorbed state of the gas has the same density as its liquid state. Molecular simulation allows the unique opportunity to view the positions of all of the gas molecules in a given slit pore, while gathering very specific data about the density and layering of the gas molecules, which may be subsequently applied to the experiments to draw further conclusions from sorption isotherms such as pore volume and pore size distribution.

To gain statistically relevant data associated with the adsorbed layer, many snapshots containing the locations of all particles were taken from different iterations. A full simulation involved running  $1 \times 10^8$  iterations, with  $5 \times 10^2$  snapshots taken ( $1 \times 10^3$  in total) equally spaced within the last  $2 \times 10^7$  iterations. The particles in all of the snapshots were aggregated and then incrementally grouped according to the particle coordinates corresponding to distance between the pore walls. Figs. 6 and 7 show one-dimensional projections of the methane density up to 18 MPa from a 3D space shown for simulations as a function of pressure. Only the axis along the width of the pore was considered, and the height of the graph reflects the number of gas molecules that have their center at the given position across the pore width, which can then be readily converted to a density given the volume element that the molecules were divided among. The dominant trend is that the majority of the methane molecules, especially at low pressures, can be found in very close proximity to the pore walls. As pressure rises, the density across the pore increases

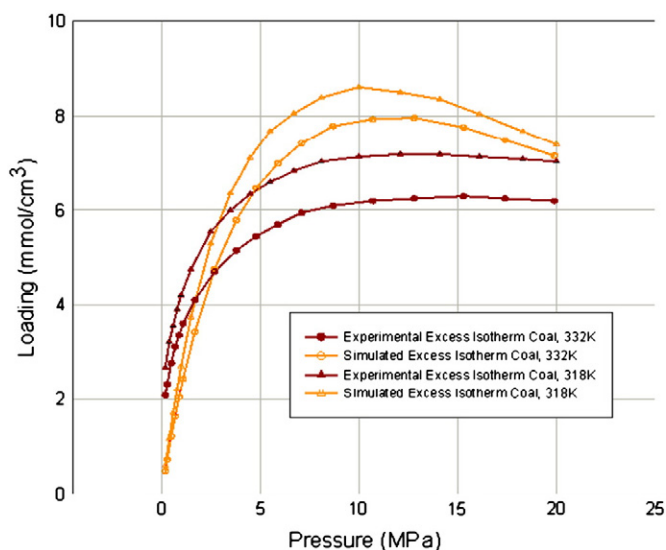


Fig. 8. Excess adsorption isotherm from simulation and experiments (Ottiger et al., 2006) at 318 K and 332 K.

generally, but with the greatest increases seen in the height and width of the first adsorption layer. Beyond the low-pressure regime, there is also clearly a second adsorption layer forming, which can be interpreted as a second peak forming after a low-density gap. This low-density gap is particularly interesting since it demonstrates that the adsorption layer is not geometrically perfect (which would force a zero density band), but that there is a clear preference to be adjacent to the pore wall. The second peak may also be interpreted to correspond with a distance roughly equal to the Lennard–Jones  $\sigma$  value, from the first peak. Finally, the density between the secondary layers, in the center of the pore exhibits a steady increase similar to the nearly linear bulk density increase with pressure as shown previously in Fig. 2.

In particular, Fig. 6 shows only the smaller pores, i.e., between 0.4 nm and 2 nm. The significantly higher peaks shown for the 0.4-nm pore are a clear result of the overlapping forces from opposing pore walls that allow for increased methane density and subsequent adsorption. The wall effects also appear to dominate over pressure effects, as the adsorbed layer is already nearly at its maximum density at 1 MPa with little change seen up to 12 MPa. The 0.6-nm sized pore has the most dramatic deviation, with much lower peaks than expected. There are clearly two layers forming, similar to the larger pores, but the layers are prevented from forming normally as is shown by the low density of the peaks. The 0.7-nm sized pore shows higher than expected density layers, but also thinner, which agrees with the non-monotonic change of methane adsorption with increasing pore width. With a 0.8-nm sized pore there is still an increase in density from the opposing pore wall effect, resulting in a slightly higher than expected density, but the layers are now the standard width as exhibited in the largest pores. The 0.9- and 1.0-nm sized pores allow for slight formation of a single central layer and both have slightly lower than the expected density. The density in the 0.9-nm sized pore is diminished since it has unoccupied space, while the 1-nm sized pore exhibits the slight formation of a central layer which creates additional space in the pore center additional gas molecules.

Fig. 7 shows only the larger pores, i.e., between 2 nm and 9 nm. It shows quite clearly that for all pores greater than 1.2 nm the maximum density exhibited at the wall is essentially the same. This holds true at both lower and higher pressures. The density of the layer at the wall increases with pressure, but two pores greater than 1.2 nm at the same pressure demonstrate nearly identical adsorption layers corresponding to the given pressure. In the case of the 1.2-nm pore, this trend deviates slightly, but once again considering the geometry of the pore and the methane diameter of 0.375 nm, four layers will not fit into a 1.2-nm sized pore, but rather there exists a single, higher central peak corresponding to a single and denser layer taking the place of two less dense secondary layers in a larger pore. Another clear pattern is the bulk phase behavior in the cores of the pores. After the second peak, all of the larger pores have a density nearly identical to one another and corresponding with the concept of bulk phase behavior at a

distance from the wall where adsorption forces based upon the proximity of the pore walls are no longer dominant.

#### 4.4. Impact of total adsorption on pore size

Based on the isotherms calculated from the molecular simulations in the current work, pore size has the capability of influencing the adsorption capacity of a given material. As a demonstrative example, consider two samples with identical pore volume but differing pore size distributions. The first consideration is surface area, i.e., for an equivalent volume of pores of smaller diameter; more pores will be required for a given volume, which corresponds to a larger total surface area. The second consideration is increased density in the adsorbed layer caused in small pores (i.e., 1.2 nm or smaller) by wall-wall interactions, allowing for an increased density in the adsorbed phase.

The surface area impact is a result of the density differences between the bulk phase and the adsorbed phase. For most pressures the adsorbed phase has a much higher density but only exists in close proximity to a pore wall. The amount of adsorbed material therefore scales directly with surface area of the pore walls, with the total amount of methane in a sample being a strong function of the amount of methane adsorbed. The effect on methane density from the overlapping force fields of the opposing pore walls can be seen in a comparison of the adsorption layer densities from Figs. 7 and 8 as shown in Table 5. At low pressures the difference is more pronounced, with the adsorbed layer nearly four times as dense in the 0.4-nm sized pore compared to the 9-nm sized pore and three times as dense as in the 0.8-nm sized pore. At higher pressures, the difference drops to 1.7 times the density of the 9-nm sized pore and 1.6 the density of the adsorbed layer in the 0.8-nm sized pore.

Combining both aspects, i.e., greater number of narrower pores (hence more surface area) in an equivalent pore volume and increased density in narrower pores and assuming that the effects are independent, the worst-case scenario comparing the densities of 0.4- and 9-nm sized pores at 1 MPa suggests that a sample consisting of 0.4-nm sized pores may contain 84 times more methane than a sample containing 9-nm sized pores, as demonstrated by the volume predictions in Table 6.

Given the potential impact micropore effects may have on adsorption capacities, and also the abundance of micropores often found in coal and shale gas samples, the consideration of pore size effects is very important for adsorption studies and predictions.

#### 4.5. Comparison of simulation to experiment

To validate the simulated data and to gauge the effectiveness of the simulation model, two adsorption comparisons were made with available experimental data from the literature (Ottiger et al., 2006) and are shown in Fig. 8.

The experimental data was collected using coal samples with a rank of high-volatile bituminous coal from the Sulcis region in Italy (Ottiger et al., 2006). The micropore size distribution for the coal was calculated based upon low-pressure CO<sub>2</sub> adsorption measurements and the Dubinin–Astakhov equation, which is based on the assumption of

**Table 5**  
Adsorption layer densities in pores with three different pore sizes (0.4 nm, 0.8 nm, and 9 nm) at 1 MPa and 12 MPa.

Condition	Density at 1 MPa (g/L)	Density at 12 MPa (g/L)
Pore size 0.4 nm	1944	2346
Pore size 0.8 nm	674	1500
Pore size 9.0 nm	520	1389
Bulk gas at 298 K <sup>a</sup>	6.59	93.2
Liquid at boiling point, 101.3 kPa <sup>a</sup>	NA	423
Methane hydrate (fire ice) <sup>b</sup>	NA	900

<sup>a</sup> Ref (Lemmon et al., 2012);

<sup>b</sup> Ref (Max, 2003).

**Table 6**  
Methane volume converted to standard temperature and pressure (STP).

Pore size (nm)	Methane at 1 MPa (scf)	Methane at 12 MPa (scf)
0.4	1609	1924
0.8	790	1631
9.0	85	581

volume filling of micropores and a single Gaussian pore size distribution. On the other hand, the simulated adsorption isotherm is calculated by:

$$\rho_{\text{simulated}}(j) = \sum_{i=1}^m a_i \rho_i(j) \quad (2)$$

such that  $a_i$  is the fraction of pores with corresponding widths. Similar to previous work, the set of isotherms for a given system were obtained from GCMC simulations (Liu and Wilcox, 2012b). From Fig. 8, the theoretical predictions deviate from experimental measurements up to 2 mmol/cm<sup>3</sup>, with increased deviation at pressures between approximately 5 and 15 MPa. There are several possible reasons for these discrepancies. The first reason is that the measured PSD does not account for the complete pore structure adsorbed by methane. The probe gas CO<sub>2</sub> may “see” different pore volumes than methane (Lowell, 2004). For instance, CO<sub>2</sub> is an adsorbing gas in porous carbons, while methane has been generally considered to be nonadsorbing. The second possible reason is the PSDs predicted are not necessarily identical to the real system due to the idealized single Gaussian pore size distribution used in the experimental-based approach. The third is due to the fact that the real organic pore structures of coal are more complex than the simplified perfect graphite slit-pore model, which includes highly structural and chemical heterogeneities that may enhance (or hinder) methane adsorption (Liu and Wilcox, 2012a, 2013). Additionally, the model predictions do not allow swelling or expansion of the pore walls, which coal has been known to exhibit. In addition, it is important to recognize that pore structure of the Sulcis bituminous coal considered might be more heterogeneous than the accepted slit-pore structure of the molecular simulations. Hence, future work will involve the investigation experimental pore size analysis on higher-ranked coals such anthracite to determine whether the pore structure may play a role in determining the extent of adsorption.

## Acknowledgments

This work was conducted with support from the Two Elk Energy Park Integrated Clean Energy Solutions Fund at Stanford University. The computations were carried out on the Center for Computational Earth & Environmental Science (CEES) cluster at Stanford University. We also thank our cluster administrator, Dennis Michael for installation of the MUSIC code on the CEES cluster. We also thank Dr. Ronny Pini for his helpful discussions and insight on this work.

## References

- Allen, M.P.T.D.J., 1989. *Computer Simulation of Liquids*. Clarendon Press.
- Benson, S.M., Orr, F.M., 2008. Carbon dioxide capture and storage. *MRS Bulletin* 33, 303–305.
- Busch, A., Gensterblum, Y., 2011. CBM and CO<sub>2</sub>-ECBM related sorption processes in coal: a review. *International Journal of Coal Geology* 87, 49–71.
- Chalmers, G.R.L., Bustin, R.M., 2007. On the effects of petrographic composition on coalbed methane sorption. *International Journal of Coal Geology* 69, 288–304.
- Cracknell, R.F., Nicholson, D., Quirke, N., 1994. A grand canonical Monte-Carlo study of Lennard-Jones mixtures in slit pores; 2: mixtures of two centre ethane with methane. *Molecular Simulation* 13, 161–175.
- Cracknell, R.F., Nicholson, D., Tennison, S.R., Bromhead, J., 1996. Adsorption and selectivity of carbon dioxide with methane and nitrogen in slit-shaped carbonaceous micropores: simulation and experiment. *Adsorption* 2, 193–203.
- Davis, S.J., Caldeira, K., Matthews, H.D., 2010. Future CO<sub>2</sub> emissions and climate change from existing energy infrastructure. *Science* 329, 1330–1333.
- Dreisbach, F., Staudt, R., Keller, J., 1999. High pressure adsorption data of methane, nitrogen, carbon dioxide and their binary and ternary mixtures on activated carbon. *Adsorption* 5, 215–227.
- Frenkel, D.S.B., 2001. *Understanding Molecular Simulation*, 2nd ed. Academic Press, New York.
- Gan, H., Nandi, S.P., Walker Jr., P.L., 1972. Nature of the porosity in American coals. *Fuel* 51, 272–277.
- Gupta, A., Chempath, S., Sanborn, M.J., Clark, L.A., Snurr, R.Q., 2003. Object-oriented programming paradigms for molecular modeling. *Molecular Simulation* 29, 29–46.
- Heuchel, M., Davies, G., Buss, E., Seaton, N., 1999. Adsorption of carbon dioxide and methane and their mixtures on an activated carbon: simulation and experiment. *Langmuir* 15, 8695–8705.
- Hoffert, M.I., Caldeira, K., Benford, G., Criswell, D.R., Green, C., Herzog, H., Jain, A.K., Kheshgi, H.S., Lackner, K.S., Lewis, J.S., Lightfoot, H.D., Manheimer, W., Mankins, J.C., Mauel, M.E., Perkins, L.J., Schlesinger, M.E., Volk, T., Wigley, T.M.L., 2002. Advanced technology paths to global climate stability: energy for a greenhouse planet. *Science* 298, 981–987.
- IEA, 2010. *Energy Technology Perspectives, Scenarios & Strategies to 2050*. International Energy Agency.
- Kurniawan, Y., Bhatia, S.K., Rudolph, V., 2006. Simulation of binary mixture adsorption of methane and CO<sub>2</sub> at supercritical conditions in carbons. *AIChE Journal* 52, 957–967.
- Lemmon, E.W., McLinden, M.O., Friend, D.G., 2012. “Thermophysical Properties of Fluid Systems” in NIST Chemistry WebBook. NIST Standard Reference Database Number 69. In: Linstrom, P.J., Mallard, W.G. (Eds.), *National Institute of Standards and Technology*, Gaithersburg MD, p. 20899 (<http://webbook.nist.gov>).
- Liu, Y., Wilcox, J., 2012a. Effects of surface heterogeneity on the adsorption of CO<sub>2</sub> in microporous carbons. *Environmental Science and Technology* 46, 1940–1947.
- Liu, Y., Wilcox, J., 2012b. Molecular simulation of CO<sub>2</sub> adsorption in micro- and mesoporous carbons with surface heterogeneity. *International Journal of Coal Geology* 104, 83–95.
- Liu, Y., Wilcox, J., 2013. Molecular Simulation Studies of CO<sub>2</sub> Adsorption by Carbon Model Compounds for Carbon Capture and Sequestration Applications. *Environmental Science and Technology* 47 (1), 95–101.
- Lowell, S., 2004. *Characterization of Porous Solids and Powders: Surface Area, Pore Size, and Density*. Kluwer Academic Pub.
- Mardon, S.M., 2008. *Evaluation of Coalbed Methane and Carbon Dioxide Sequestration Potential in the Western Kentucky Coalfield*, The Graduate School. University of Kentucky.
- Martin, M.G., Siepmann, J.I., 1998. Transferable potentials for phase equilibria. 1. United-atom description of n-alkanes. *The Journal of Physical Chemistry*. B 102, 2569–2577.
- Max, M.D., 2003. *Natural Gas Hydrate in Oceanic and Permafrost Environments*. Kluwer Academic Publishers, Boston.
- Moore, T.A., 2012. Coalbed methane: a review. *International Journal of Coal Geology* 101, 36–81.
- Müller, E.A., Gubbins, K.E., 1998. Molecular simulation study of hydrophilic and hydrophobic behavior of activated carbon surfaces. *Carbon* 36, 1433–1438.
- Müller, E.A., Rull, L.F., Vega, L.F., Gubbins, K.E., 1996. Adsorption of water on activated carbons: a molecular simulation study. *Journal of Physical Chemistry* 100, 1189–1196.
- Müller, E.A., Hung, F.R., Gubbins, K.E., 2000. Adsorption of water vapor-methane mixtures on activated carbons. *Langmuir* 16, 5418–5424.
- Ottiger, S., Pini, R., Storti, G., Mazzotti, M., Bencini, R., Quattrocchi, F., Sarđu, G., Deriu, G., 2006. Adsorption of pure carbon dioxide and methane on dry coal from the sulcis coal province (SW Sardinia, Italy). *Environmental Progress* 25, 355–364.
- Reid, R.C., Prausnitz, J.M., Poling, B.E., 1987. *The Properties of Gases and Liquids*, 4th ed. McGraw-Hill Book Company.
- Ross, D.J.K., Bustin, R.M., 2009. The importance of shale composition and pore structure upon gas storage potential of shale gas reservoirs. *Marine and Petroleum Geology* 26, 916–927.
- Sing, K.S.W., Everett, D.H., Moscou, L., Pierrotti, R., Quérolo, J., Siemienińska, T., 1985. IUPAC recommendations. *Pure and Applied Chemistry* 57, 603–619.
- Steele, W.A., 1973. Physical interaction of gases with crystalline solids. 1. Gas-solid energies and properties of isolated adsorbed atoms. *Surface Science* 36, 317–352.
- Wilcox, J., 2012. *Carbon Capture*. Springer Publishing, New York.
- Zhang, T., Ellis, G.S., Ruppel, S.C., Milliken, K., Yang, R.S., 2012. Effect of organic-matter type and thermal maturity on methane adsorption in shale-gas systems. *Organic Geochemistry* 47, 120–131.